# Micro-Texturing for Tribology and Surface Engineering in Manufacturing Processes

Tatsuhiko Aizawa
Department of Engineering and Design, Shibaura Institute of Technology
3-9-14 Shibaura, Minato-City, Tokyo 108-8548, Japan

**Abstract:** The friction and wear has been understood as the mechanical and chemical issues on the surface and interface between structural components and parts with the practical surface roughness. The micro-texturing was highlighted as a positive use of interfacial asperities in geometry and topology to control the frictional behavior. Three micro-texturing methods were proposed to control the micro-texture size and geometry; i.e., the self-micro-texturing, the extremely short pulse laser micro-texturing, and, the plasma printing. The ball-on-disc testing was employed to describe the effect of micro-dimple size, density and topology on the measured friction coefficient. The wear track width was also measured to investigate the effect of micro-dimples on the wear. The surface properties were affected by the micro-textures on the surface. The static contact angle was measured to describe the effect of micro-texture size and topology on the increase of contact angle toward hydrophobicity. The micro-textured surface of aluminum sheets by the plasma printing was utilized to investigate the controllability of heat transfer processes by the micro-texturing.
**Keywords:**

## 1. Introduction

In the manufacturing process, the lubricating oils have been utilized to be working as an interfacial buffer between the tools and the work materials to reduce the wear and friction in practice. With consideration on the surface roughness of tools and works in nature, this lubricating behavior was described by the applied load (W) and the shearing velocity (v) in the tool-work system as well as the viscosity (η) of lubricating oils. The Stribeck curve as shown in Fig. 1 was a typical relationship between the friction coefficient (μ) in the tool-work system and the mechanical parameter ϕ. This ϕ was usually defined by v x η / W after[1)].

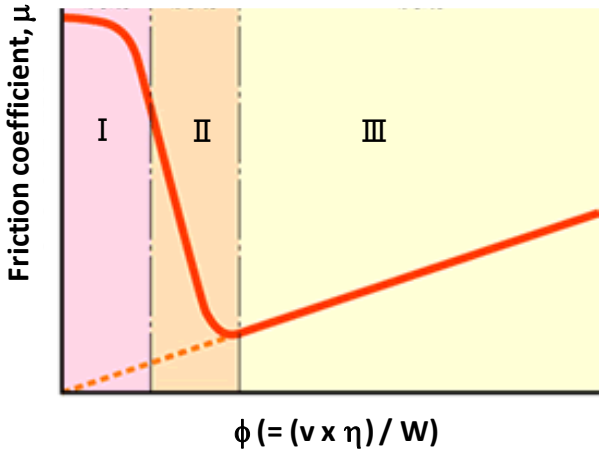


Fig. 1.1. A typical Stribeck curve between the friction coefficient and the lubricating parameter ϕ (= (v x η) / W).

The tribology in the machining or cutting processes was usually classified into the region I in Fig. 1.1 In this boundary lubrication condition, the lubricating oil film was too thin to preserve the well-defined lubricating conditions. Most of metal forming processes were categorized from the region II to the early stage of region III. With increase of ϕ, the friction coefficient reduced monotonically and minimized on the border between these two regions; the friction coefficient

increased with increase of the lubricating oil thickness. This typical tribological behavior stands on the topological configuration of interface between tool and work surfaces. Hence, the above tribological behavior must be changed by micro-texturing onto the work surface[2)] or onto the die or tool surfaces[3, 4)].

With decreasing the size of products, the fresh surface area significantly increased in the machining, stamping and forging processes. In particular, the surface area extension rate often exceeded 10 or 20 in correspondence to highly frictional process in the severe press-forging steps. In addition, the recent regulations for reduction of environmental burdens and material emission recommended a new direction to utilize the low-viscosity natural oils under minimum quantity lubrication (MQL). Hence, without significant innovation to control the lubricating process, $\phi$ could be smaller enough to increase the friction coefficient in micro-manufacturing. The engineered surface design was also high-lighted, both in the control of wettability by micro- and nano-texturing[5)], and, on the control of heat transfer processes through the tailored surfaces[6)]. In the former, the geometry and topological alignment of micro-textures must be optimized to increase the contact angle toward hydrophobicity. In the latter, the micro-textures were expected to reduce the vapor bubble size and release those tiny bubbles from the heated surface.

Authors have been concerned with the micro-texturing methods for applications in the above. As the first method, the self-micro-texturing method[7)] was proposed to modify the surface conditions by using the low temperature plasma nitriding. The original smooth surface changed itself to the roughed one with micro-dimples via nitriding. The extremely short-pulse laser micro-texturing[8,9)] was the second approach to form each micro-dimple with high geometric accuracy by laser machining and to align this micro-dimple assembly by controlling the laser-paths. The plasma printing method[10-11)] was developed to form the micro-dimples as a micro-mold as well as the micro-pillars as a micro-punch onto the die surface. The micro-pillared plastic specimens were fabricated by injection molding even into those micro-molds. The micro-dimpled metallic sheets were fabricated by micro-stamping this multi-punched die in a single shot.

In the present paper, how to make micro- and nano-texturing into tools and dies is reconsidered with importance on the characteristic procedures for three methods as stated in the above: i.e., the self-micro-texturing, the extremely short-pulse laser micro-texturing, and, the plasma printing. The first two methods are employed to describe the effect of micro-dimple size, density and topology on the frictional behavior under MQL. The ball-on-disc method is employed to measure the time variation of friction coefficient for the micro-dimpled stainless steels with comparison to the bare substrates. The third method is first utilized to make a die with micro-mold patterns on its surface by the plasma printing method and to prepare for the micro-pillared plastic specimens. Those test-pieces are used to measure the contact angle for the pure water and to investigate the effect of micro-mold size and topology on the increase of contact angle toward hydrophobicity. This plasma printing is further used to form the micro-punched die for fine stamping. The micro-dimpled aluminum sheets are fabricated as a specimen to investigate the effect of micro-punch size and geometry on the heat transfer process.

## 2. Micro- and Nano-Texturing Methods

There are three ways to form the micro-textures on the product and tool surfaces and interfaces by the micro- and nano-texturing. The first approach is a natural self-texturing method where the fine, distributed micro-dimples are naturally formed through the surface treatment. In the low temperature plasma nitriding of stainless steels and tool steels, the interstitial nitrogen atoms diffuse into the depth of steels together with their occupation of octahedral and tetrahedral vacancy sites in the iron/chromium crystalline bcc-lattice structure. This occupation takes place together with the lattice expansion of stainless steel crystals significantly in the c-axis. Each grain in the depth of nitrided layer from the surface expands itself and is subjected to straining against other grains. The grains at the vicinity of substrate surface expand also in the c-axis and deform toward the free surface. The surface areas in vertical to the c-axis expand by themselves together with the above lattice expansion; the other ones in parallel to the c-axis never expand, or, a little contract by themselves. This disturbance in the surface deformation results in roughing with formation of micro-dimples. Fig.2.1. compared the change of surface conditions before and after the low temperature plasma nitriding at

693 K for 14.4 ks. Fine micro-dimples are uniformly formed to be working as an oil-pocket in the lubricated tribology even under MQL.

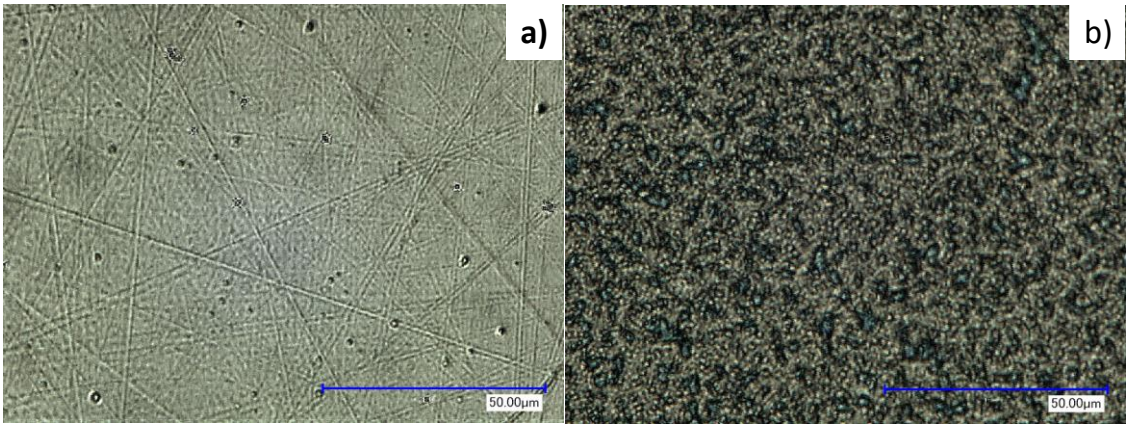


Fig. 2.1. Self micro-texturing process to form the surface roughing process in nature. a) The bare stainless steel surface of type AISI-SUS420J2, and, b) the low temperature plasma nitrided surface at 693 K for 14.4 ks.

The extremely short pulse laser machining provides a means to make any tailored alignment of micro-dimples via the artificial control of laser powers and paths. Different from the conventional $CO_2$-lasers or the fiber lasers, the pico-second or femto-second pulse laser machining processes are free from the thermal effects; every fine groove or dimple is formed onto the work surfaces and interfaces only by ablation process of the work materials. This results in accurate formation of the micro-dimples even onto the hard metallic and ceramic substrates. In the following experiments, the whole positioning data, related to the geometries for all the micro-dimples, must be prepared together with the laser power and path data and edited into the CAM data before actual laser machining. Each micro-dimple is formed step-by-step by controlling the laser path.

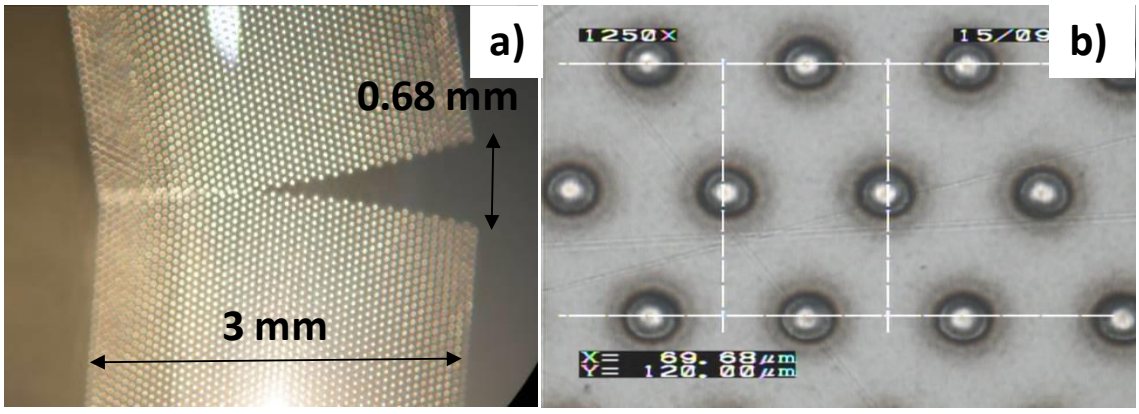


Fig. 2.2. Extremely short pulse laser micro-texturing into any materials. a) Laser-micro-textured die inlet for deep drawing, and, b) Geometric dimension of aligned micro-dimples by the laser-micro-texturing.

Fig. 2.2. depicted the laser micro-textured die inlet surface by using the pico-second pulse lasers. Each micro-dimple is accurately machined into the die surface even when the micro-dimple size becomes equivalent to its grain size. Its geometric alignment is also accurate to have a capacity to preserve the thin, uniform oil films in lubrication.

The micro- and nano-texturing by the plasma printing method has two independent procedures to form the micro-textured dies and molds. The first plasma printing method consists of three steps, as illustrated in Fig. 2.3. In Fig. 2.3 a), the solid circle pattern is ink-jet printed directly onto the stainless steel mold surface. Its size and geometry in this two dimensional micro-pattern corresponds to the outlet size and geometry of micro-texture. This micro-pattern is utilized as a mask to prevent the micro-patterned surface area from the plasma nitriding. The bare mold surface is plasma-nitrided to have higher hardness than the masked surfaces. After this second step in Fig. 2.3. b), the masked area with the same hardness as the bare stainless steel mold is mechanically removed by the sand

blasting as shown in Fig. 2.3. c). This micro-dimpled mold is fixed into the mold-set for injection molding. Through this molding process, the micro-disc or micro-pillar textures are formed onto the plasmatic product surfaces by transcription of the micro-dimple textures on the mold.

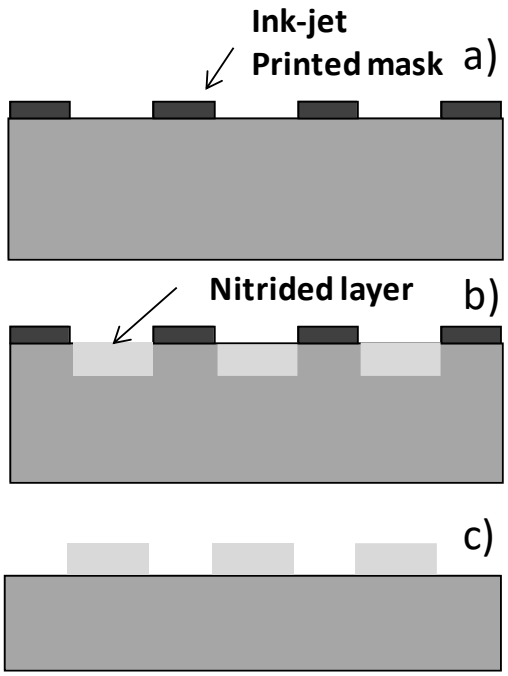


Fig. 2.3. The plasma nitriding-assisted printing to the stainless steel molds for injection molding of the polymer and plastic products with micro-textures.

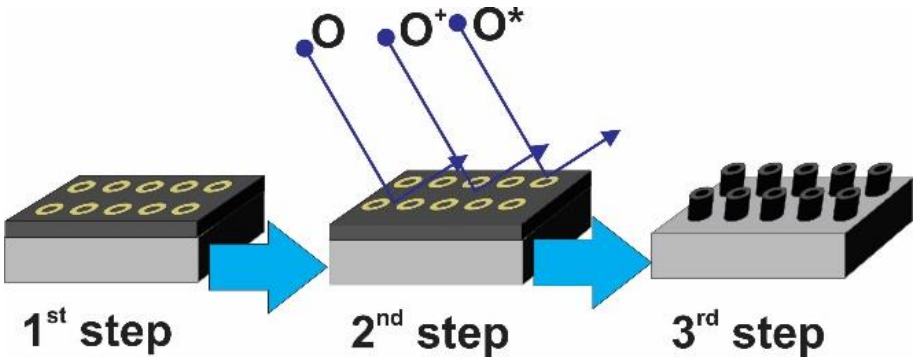


Fig. 2.4. The plasma oxidation-assisted printing to the DLC coated dies for fine micro-stamping of the metallic sheets with micro-textures.

In the second procedure, the oxygen plasmas assist this printing process into DLC-coated dies. Just in the similar manner to Fig. 2.3. a), the initial two-dimensional pattern is ink-jet printed as a mask to prevent the masked area from plasma oxidation as illustrated in Fig. 2.4. The bare DLC coating area is removed to build up the DLC-micro-punches directly into the DLC-coated dies. This die unit is inserted into a cassette die for micro-stamping of the aluminum sheet. Through this micro-stamping, the micro-cavities are formed into the aluminum sheet by transcription of the DLC-micro-punch shapes.

### 3. Micro-Texturing Effects on the Friction and Wear

The ball-on-disc tribometer (CSM-Instrument, Co. Ltd.) was employed to describe the history of friction coefficient with the sliding distance. The applied load was constant by 10 N, and, the sliding velocity, 10 cm/s. Toward the green manufacturing under MQL, the spindle-oils were only supplied by 0.1 ml at the initial condition. The SUJ2 ball with the diameter of 6 mm was used as a counter material. As illustrated in Fig. 3.1, the tribo-testing can be done in dry, in semi-dry or in lubricating conditions. The frictional force (F) was in-situ measured for the applied load (W); the fictional coefficient was determined by F/W in the function of time.

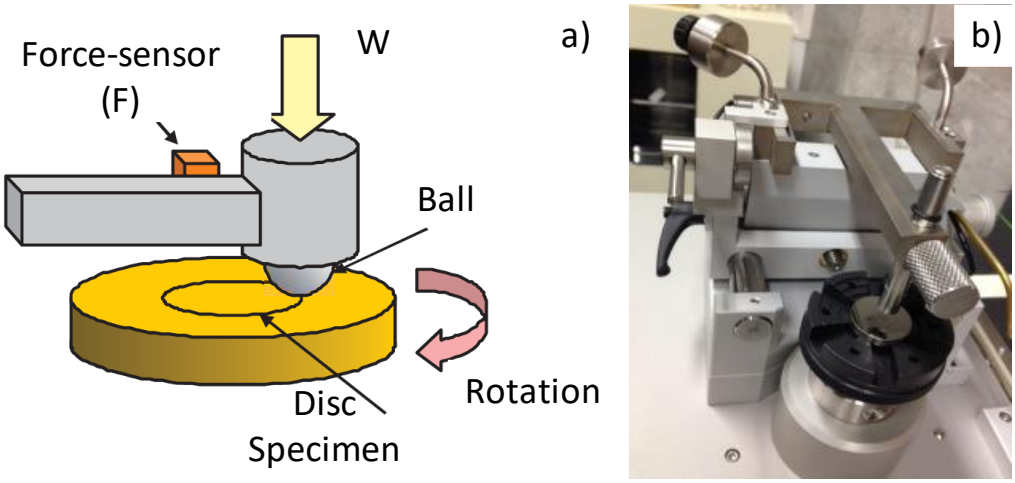


Fig. 3.1. Illustration of the ball-on-disc method to evaluate on the time variation of the friction coefficient in MQL conditions. a) Mechanism of the present ball-on-disc tribo-testing, and, b) The ball-on-disc tribo-meter.

Both the bare and the self-micro-textured stainless steel disc specimens with the diameter of 25 mm and the thickness of 5 mm were prepared for the tribo-testing under MQL. In both cases, the spindle oils were deposited by 0.1 ml at the beginning of test. Fig. 3.2 compared their time variation of measured friction coefficient ($\mu$). In case of the bare specimens, the friction coefficient fluctuated continuously above $\mu = 0.1$ by the metallic contact between the worn fresh surface of specimen and the hard ball surface. This implies that the friction process should be enhanced by the adhesive wear of specimen with increasing the tribo-testing time. On the other hand, little fluctuations or no increase of the friction coefficient was seen for the self-micro-textured specimen; e.g., $\mu = 0.1$ was preserved through the whole tribo-testing time for 3.6 ks. This difference reveals that the self-structured micro-dimples on the low temperature plasma nitrided surface should work as an oil pocket to preserve the thin lubricating oil layer enough to prevent the test-piece surface from direct contact with the hard counter balls.

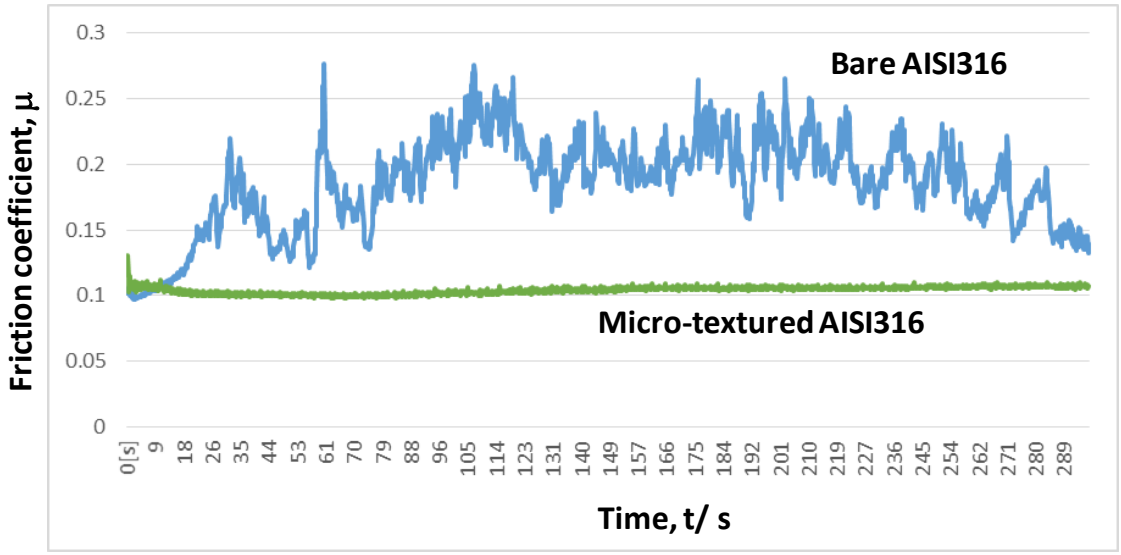


Fig. 3.2. Comparison of the time variation of friction coefficient between the bare AISI-SUS316 and the self-micro-textured AISI-SUS316.

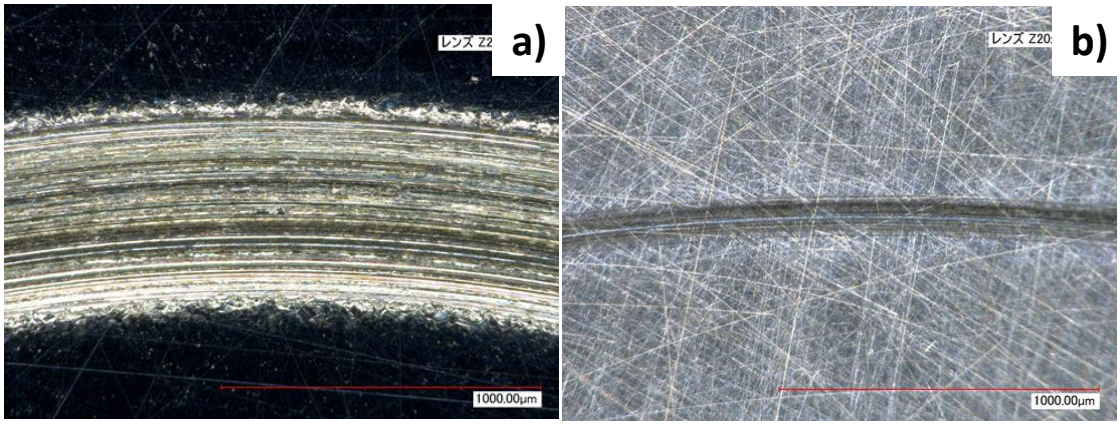


Fig. 3.3. Comparison of the wear tracks after tribo-testing between the bare AISI-SUS316 and the nitride AISI-SUS316.

Fig. 3.3. also compared the wear tracks after tribo-testing between the bare and the self-micro-textured stainless steel disc specimens of type AISI-SUS316. The bare specimen experienced severe wear as shown in Fig. 3.3. a). This deep wear track width of 630 μm was significantly reduced to 135 μm for the self-micro-textured specimen in Fig. 3.3. b). This reduction of friction and wear by self-micro-texturing reveals the important role of micro-textures in the tribology in manufacturing.

The laser micro-texturing with use of the pico-second lasers was employed to form the assembly of micro-dimples onto the surface of martensitic stainless steel type AISI420. Different from the self-micro-texturing, this method requires for each micro-dimple geometry and positioning information as CAM data. Each micro-dimple is formed with accurate size, depth and alignment. Fig. 3.4. a) depicted a typical micro-textured specimen with the diameter of 25 mm and the thickness of 5 mm. As shown in Fig. 3.4. b), each micro-dimple was formed to have 30 μm in diameter and 3 μm in depth.

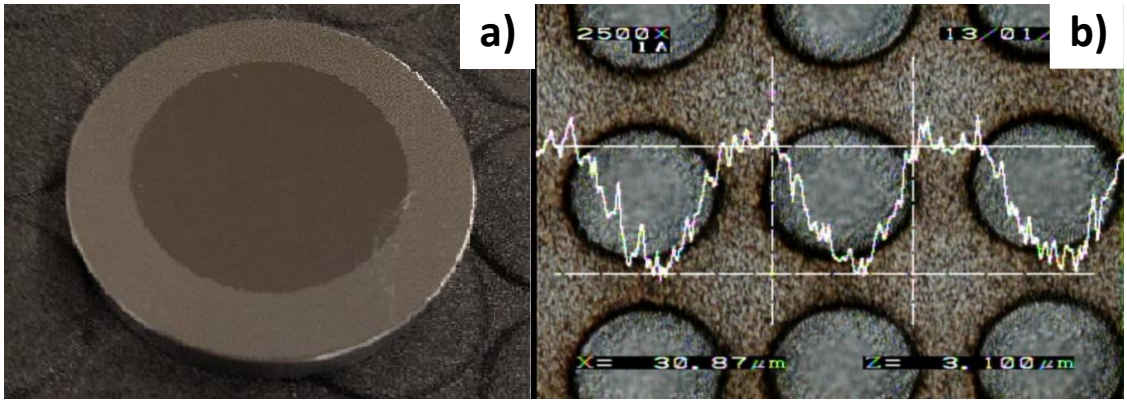


Fig. 3.4. The micro-textured disc specimen. a) Micro-texturing at the center of specimen, and, b) SEM image of textured micro-dimples with the surface profiles.

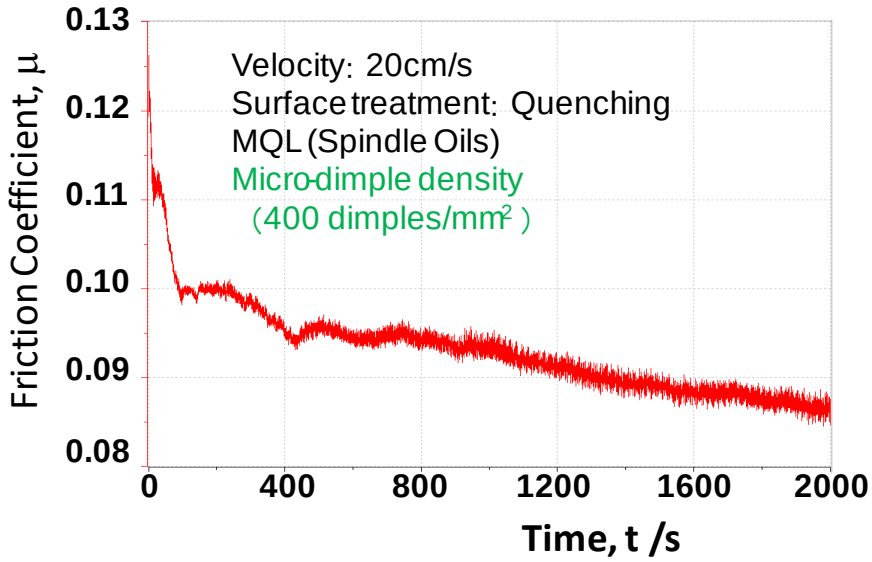


Fig. 3.5. Time variation of the measured friction coefficient for the micro-textured disc specimen by the laser micro-texturing.

Fig. 3.5. depicted the time variation of measured friction coefficient in the tribo-testing. Every micro-dimple has the same dimensions in geometry as stated in the above. This micro-dimple alignment has the density of 400 dimples / $mm^2$. Excluding the initial running out, the friction coefficient gradually decreased from 0.1 to 0.085 with time. This monotonic reduction of the friction coefficient must be driven by formation of the thin lubricating layer from the micro-dimples. At the beginning, the ligaments among the micro-dimples have discontinuous oil films; higher frictional forces are applied to the specimen. Since the thin oil films gradually grow into a continuous thin film from the micro-dimples, the friction coefficient is reduced in time. This monotonic reduction of the friction coefficient also implies that every micro-dimple in the contact track with the counter ball should work as an oil pocket to keep thin and homogeneous oil film between the specimen surface and the counter balls. Once some micro-dimples were worn out in the contact track, the friction coefficient could be fluctuated noticeably.

In order to prove this role of micro-dimples in lubrication, the wear track was measured on the specimen by SEM. Fig. 11 depicted the wear track on the micro-textured specimen surface. The wear track width was only 100 μm. All the micro-dimple sizes in this contact track remain the same or a little smaller than the average size of micro-dimples before testing. Since the diameter of ball is 6 mm, the indentation of counter ball is estimated to be shallow by 0.4 μm. This elastic contact state between the counter ball and the micro-textured surface must be preserved at the presence of thin oil films from micro-dimples.

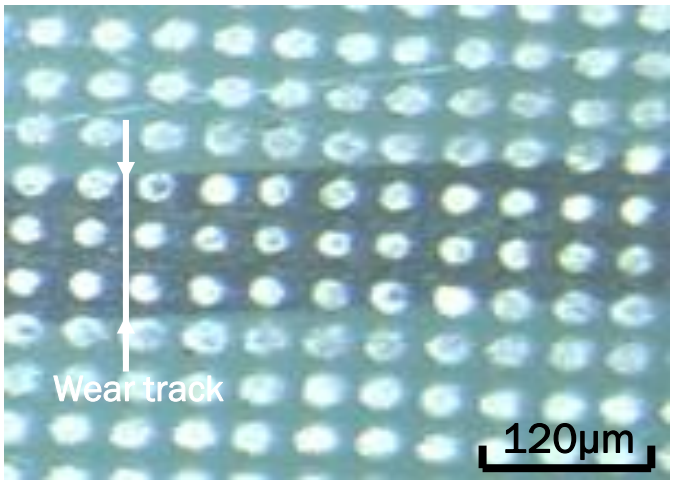


Fig. 3.6. The wear track of micro-textured specimen surface after the tribo-testing.

This lubricating role of micro-dimples on the specimen surface has a potential to reduce the friction coefficient in the transient zone from the region II to the region III in Fig. 1.1. Let us summarize the relations between the friction coefficient and the sliding velocity for each micro-texturing condition. In this experiment, the applied load was constant, and, the same spindle oil was used. Then, Fig. 3.7. compares the Stribeck curve for each micro-texturing condition. Irrespective of the pitch among the micro-dimples with the diameter of 50 μm, the friction coefficient was reduced from 0.13 - 0.16 for the bare specimens to 0.08 with increasing the micro-dimple density.

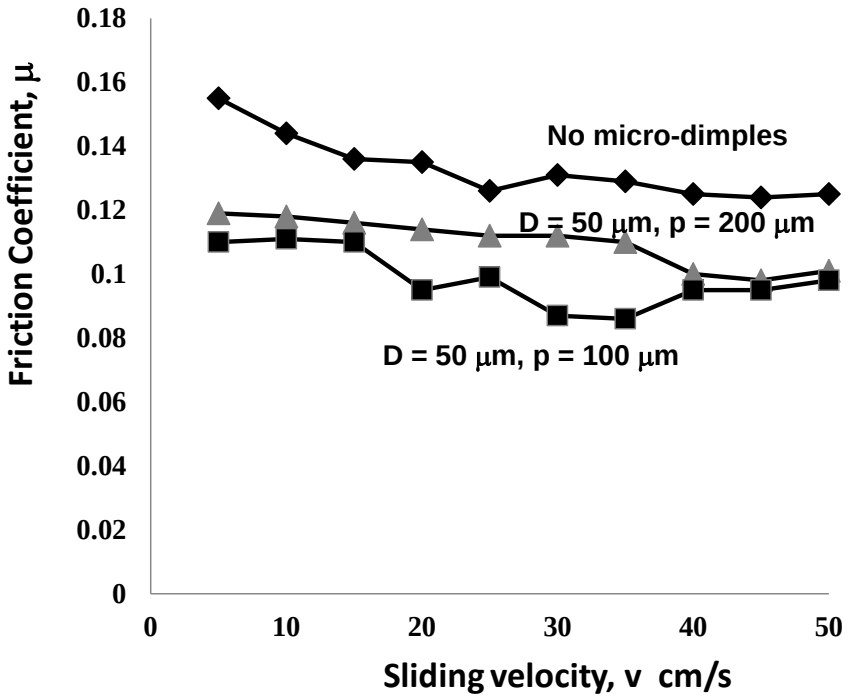


Fig. 3.7. The role of the micro-dimple texturing on the Stribeck curves in the lubrication.

## 4. Micro-/Nano-Texturing Effects on the Surface Properties

The surface properties of materials are governed by the surface energy. For an example, the high energy surface is easy to be covered by atom or molecule layers so that the surface becomes hydrophilic and easy to be wet. The low energy surface has lower attractive capacity to other material atoms and molecules; they usually agglomerate themselves to be isolated from the surface. This hydrophobic surface is difficult to be wet. In the usual way, this hydrophobicity is accommodated by the fluorine coating; the measured contact angle turns to be 130 to 150[12]. In recent, this contact angle is tunable from 10° to 150° by appropriate selection of chemical agents[13]. The other way to attain this hydrophobicity lies in the usage of the lotus effect where the finely aligned thin fibers grown on the lotus leaf preserve the water droplets just above the leaf surface at the presence of air layer below fibers. This suggests that the wettability of materials surface could be controlled by micro-texturing.

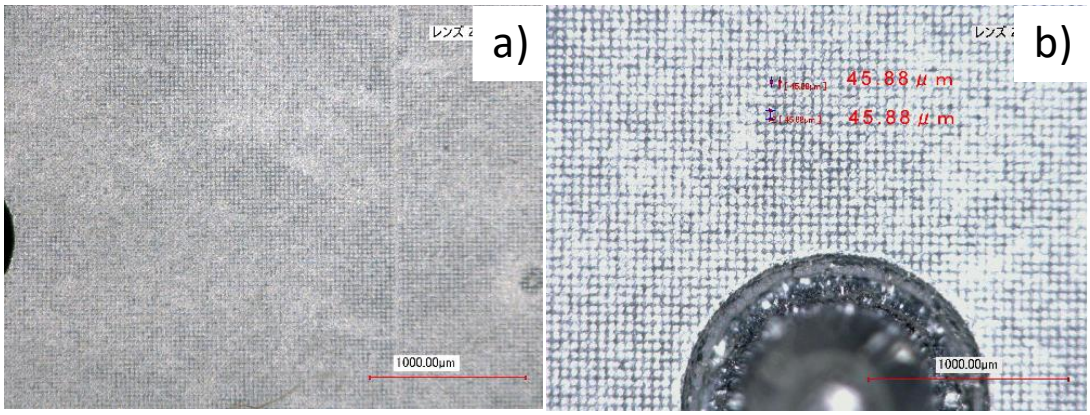


Fig. 4.1. The plasma printed mold for injection molding. a) Microscopic image of the micro-textured mold, and, b) Microscopic image of the plastic product surface molded.

The plasma nitriding-assisted printing method was first employed to make micro-structuring into the stainless steel mold for injection molding. As explained in detail by[10, 14-15], the initial two dimensional micro-patterns were ink-jet printed as a masking pattern onto the surface of martensitic stainless steel substrate type AISI420J2. During the lower temperature plasma nitriding than 700 K, no chromium nitrides precipitated in the stainless steel matrix, but, the interstitial nitrogen atoms diffused into the matrix with occupation of the tetrahedral and octahedral vacancy sites in the Fe/Cr crystalline bcc-lattice by nitrogen solute. This nitriding took place selectively on the masked surface areas; the hardness of masked area in the matrix increased up to 1400 HV. The other unmasked area on the surface had nearly the same hardness as the matrix of 250 HV. Then, those surface areas were selectively removed and polished by sand-blasting method. Fig. 4.1. a) depicted the plasma printed mold for injection molding. Micro-dots with the average diameter of 25 μm were regularly aligned on the mold surface. This micro-dot pattern was transcribed to the micro-pillar pattern by the injection molding as shown in Fig. 4.1. b).

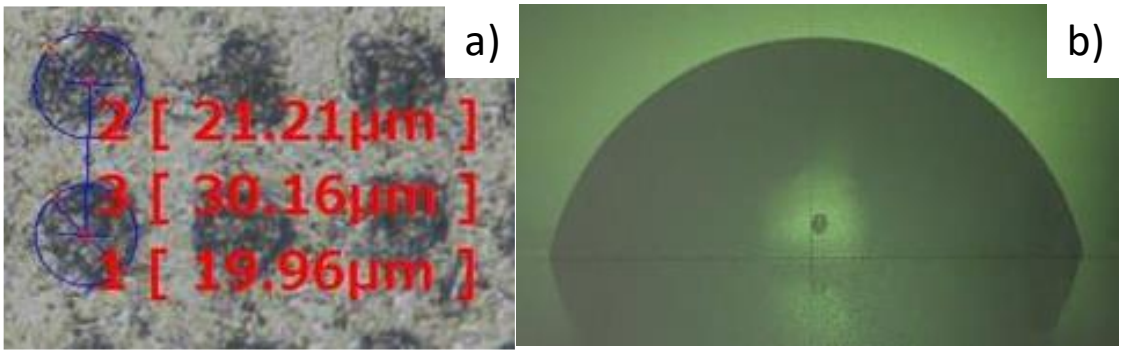


Fig. 4.2. Micro-pillar pattern on the plastic product with the normal deviation of pillar diameter from 20 to 30 μm. a) Micro-texture pattern on the product, and, b) Wettability on the micro-pillared plastic surface.

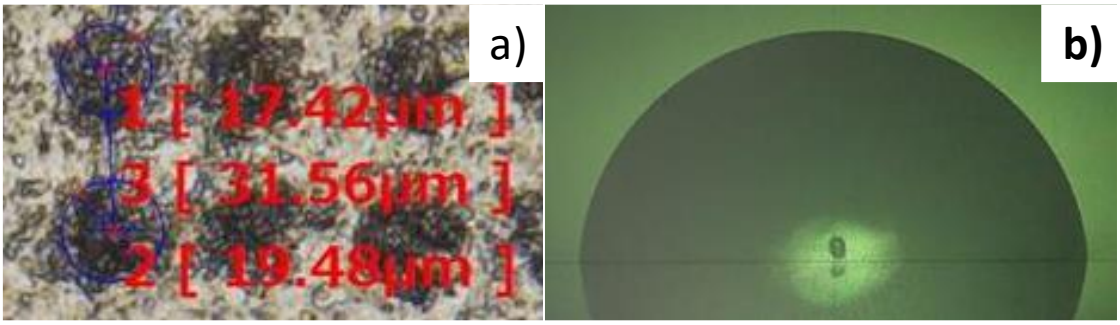


Fig. 4.3. Micro-pillar pattern on the plastic product with the normal deviation of pillar diameter from 17 to 32 μm. a) Micro-texture pattern on the product, and, b) Wettability on the micro-pillared plastic surface.

Two plastic specimens were prepared by the injection molding with used of the micro-dimpled mold unit. The first specimen has the micro-pillar textures with the deviation of diameter from 20 to 30 mm, as shown in Fig. 4.2. a). In the second specimen, this deviation is forced to be broaden to be from 15 to 32 mm, as depicted in Fig. 4.3. a). The measured static contact angle was only 70° in the first specimen; while it was improved to 85°, as respectively shown in Fig. 4.2. b) and Fig. 4.3. b). This reveals that the irregularity in the micro-textures controls the local contact area of pure water and that the contact angle increases with this local irregularity on the micro-pillared surface.

## 5. Micro-/Nano-Texturing Effects on the Heat Transfer Processes

How efficiently the generated heat is transferred out of the system, has been and is still one of the most difficult issues in engineering. The high holding temperature is necessary to activate the heat radiation process owing to the Boltzmann law[16]. As illustrated in Fig. 5.1. a), without the resonance device to red or ultra-red components in the radiated waves[17], there might be no possibility to drive this heat radiation process at the room temperature. In order to drive the heat convection process, the cool water is indispensable to improve the heat flux transferred from the hot spots; e.g., the heat sink is a typical element to increase the heat penetration rate through its finned surface[18]. However, the maximum heat flux through this element is limited by the critical heat flux where the vapor bubbles combine themselves into a vapor film. Hence, without the engineered surface to prevent the vapor bubbles from adhesion on the heated surface, there might be also little possibility to increase the heat flux above the criticality, as also illustrated in Fig. 5.1. b).

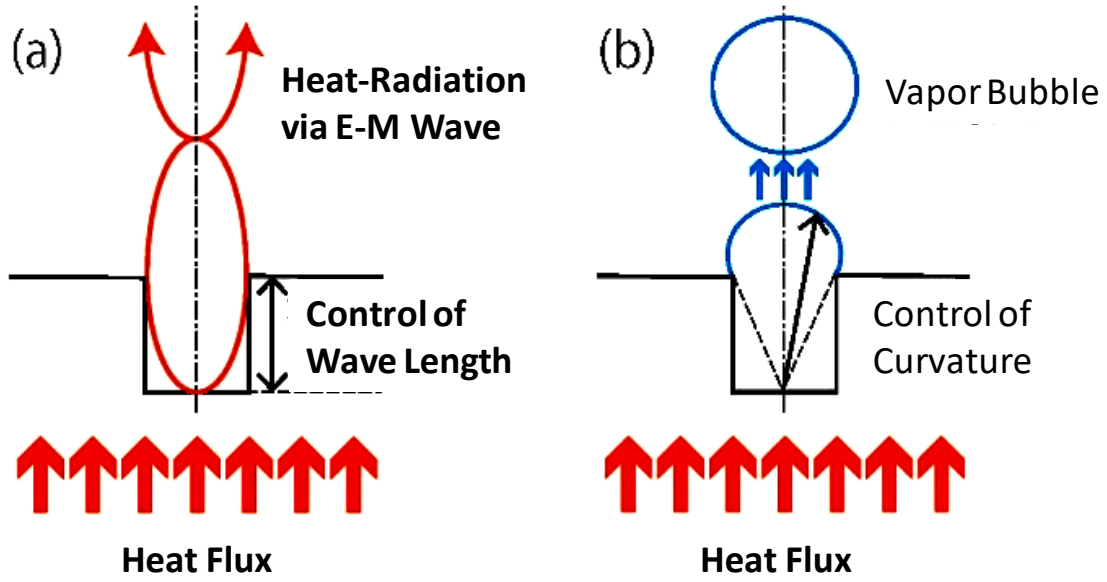


Fig. 5.1. Enhancement of the heat transfer mechanism by the micro-texturing. a) Enhancement of heat radiation mechanism at room temperature, and, b) Enhancement of the two-phase heat transfer mechanism with boiling.

The DLC-coated SKD11 substrate with 10x10x80 $mm^3$ was prepared as the starting die material. As described in detail by[11, 19-21], the micro-pillared DLC-punches were plasma printed into the DLC-coating. Each micro-pillar was shaped into the rectangular punch with 3.5 x 3.5 x 4.8 $\mu m^3$ and aligned with each other under the mutual clearance of 1.5 μm. Consider that a single rectangular DLC-punch stands on each 5 x 5 $\mu m^2$ local surface of the whole die surface with 10 x 80 $mm^2$; then, 30-mega (30,000,000) DLC multi-punches were present on the die-unit surface. This die unit was fixed into the cassette die system for CNC micro-stamper to make coining of the aluminum sheet with the thickness of 80 μm. The micro-textured aluminum sheet was shown in Fig. 5.2. As depicted in Fig. 5.2 b), each micro-cavity with 3.5 x 3.5 x 4.8 $\mu m^3$ was formed into the aluminum sheet in correspondence to the DLC micro-pillared punch. The bottom surface with 3.5 x 3.5 $\mu m^2$ of micro-cavity corresponds to the DLC-punch head; the walls of micro-cavity with the thickness of 1.5 μm, the clearance between the adjacent DLC micro-punches.

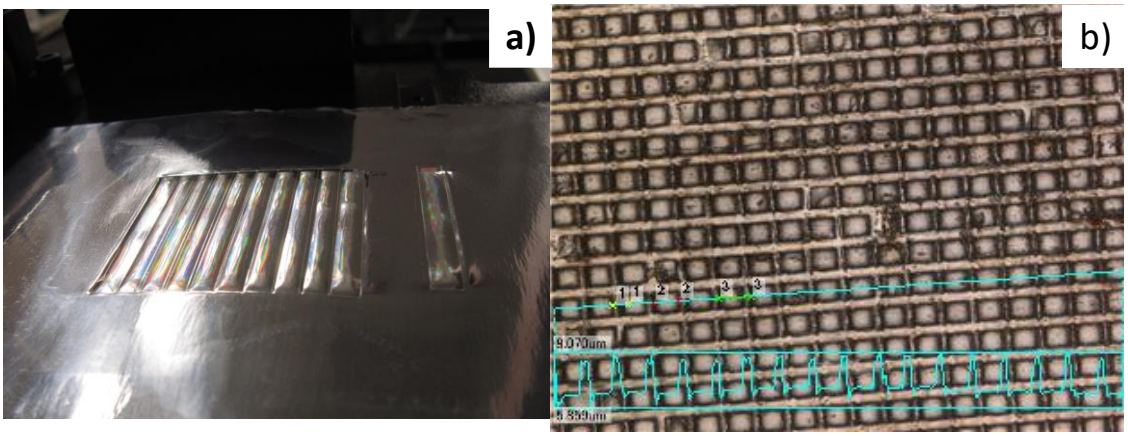


Fig. 5.2. Micro-textured aluminum A1060 alloy sheet with the thickness of 0.08 mm. a) Continuously stamped sheet with the micro-textured patterns, and, b) SEM image of the stamped micro-textures into the aluminum sheet.

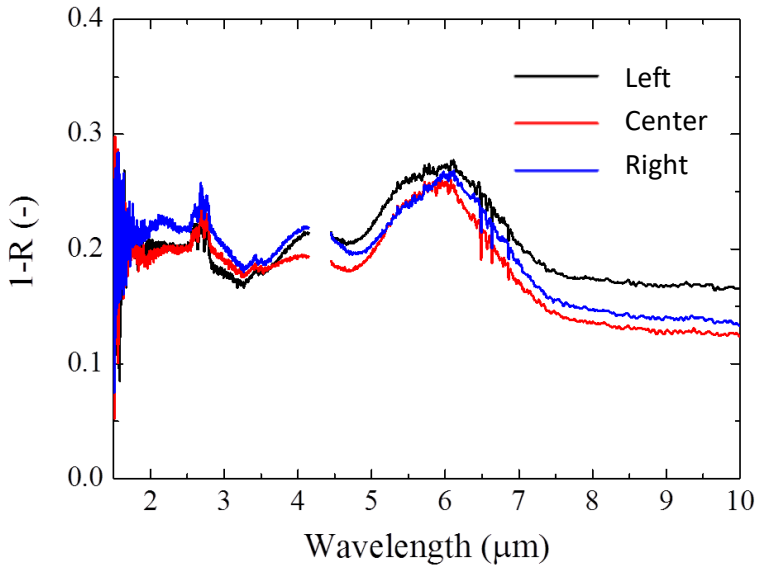


Fig. 5.3. Variation of the measured thermal radiation coefficient with the wave length for three sections in left, at center and in right on the micro-textured aluminum sheet.

The optical spectroscopy up to 9 μm was employed to measure the thermal radiation coefficient for three parts in the micro-textured aluminum sheet. Fig. 5.3. depicted the measured thermal radiation coefficient spectra for three sections in left, at center and in right on the micro-textured aluminum sheet. Their peak intensity is enhanced in the wave length from 5 to 7 μm; the heat is radiated as a red light from the micro-textured aluminum sheet.

This micro-textured aluminum sheet was joined with the copper block to be directly heated in the heat

transfer testing. In general, the heat flux (q) from the heated copper block to the water increases with the excess temperature ($\Delta T$) since more vapor bubbles nucleate on the copper block surface after free heat convection. Approaching to the critical condition where the growing vapor bubbles are combined into a vapor film, the heat flux reaches to its maximum before burning-down. Let us compare the measured heat fluxes between the bare and micro-textured aluminum sheets, joined onto the copper block in experiments.

Table 5.1. Comparison of the measured heat fluxes between the bare and micro-textured aluminum sheets. In the same experimental set-up, both sheets were joined onto the copper block in the similar way.

| **Excess Temperature $\Delta T$, K** | **Heat flux through the bare aluminum sheet $q_{bare}$, W/m$^2$** | **Heat flux through the micro-textured aluminum sheet $q_{micro}$, W/m$^2$** |
|---|---|---|
| **40** | **$0.8 \times 10^5$** | **1.0 x 105** |
| **60** | **$0.85 \times 10^5$** | **$3.2 \times 10^5$** |
| **80** | **$1.0 \times 10^5$** | **$4.0 \times 10^5$** |

As listed in Table 5.1, the measured heat flux still increases monotonically with $\Delta T$ in both cases. The heat flux of the micro-textured aluminum sheet becomes four times higher than that of the bare aluminum sheet in the higher excess temperature. This experiment directly demonstrates that the micro-textured surface provides a means to increase the heat flux without adhesion of vapor bubbles onto the heated surface and without the morphological change of this vapor bubble to vapor film.

## 6. Discussion

The thin lubricating oil film is present on the interface between the micro-textured substrate and the counter materials. Without the micro-textures, a part of oil film could be forced to squeeze out by the reactive pressure between two bodies; then, the friction coefficient increases by itself since the part of film becomes too thin to support this pressure. At the presence of micro-dimples on the contact surface between two bodies, this local disturbance of film thickness is compensated by small flush out of lubricating oils from the micro-dimples. The lubricating oil film thickness is preserved to be uniform and thin enough to sustain the pressure distribution on the contact interface. With decreasing the density of micro-dimples in the contact track, this compensation of oil film thickness in local does not work well and results in the local metal contact between two bodies. The sufficient micro-dimple density as well as its well-defined geometric configurations, are indispensable to lower the friction and wear, irrespective of the sliding velocity and the applied load.

Without micro-grooves on the surface, the wettability of materials against the pure water is uniquely determined by the surface energy of substrate; e.g., the bare stainless steel has contact angle as low as 20 - 30$^o$. At the presence of micro-grooves or micro-discs in the order of 10 to 30 μm with relatively accurate alignment, this contact angle is increased up to 70$^o$. With increase of the deviation in the micro-disc diameter, it further increases more than 80$^o$. This result suggests that the contact angle should be enhanced by tailoring the local alignment of micro-groove and micro-disc units. Through the spatial frequency analysis on the tailored micro-texture surface, the optimum alignment of micro-texture units is investigated to search for the rational design of engineered surface toward the super-hydrophobicity.

In the heat radiation device with use of the micro-textures, the deep rectangular micro-cavity structure is needed to build up the micro-resonator with the half wave length for red and ultra-red waves. At present, the depth of micro-cavity is limited by the DLC micro-punch of 5 μm. Using the thick DLC films up to 20 to 30 μm as a die material, feasible resonating microstructure is fabricated into the metallic sheet. With respect to the heat transfer with two-phase condition, there is no theoretical treatise on the optimum micro-texture configuration. Refinement of vapor bubbles as well as prompt separation of vapor bubbles from the heated surface must be accommodated to new heat transfer process by the micro-texturing design to increase the heat flux above the criticality.

## 7. Conclusion

Tribology has grown up to describe the lubricating behavior on the smooth surfaces in contact with natural roughness. Its fundamental property and performance changes itself on the micro-textured surfaces in contact. The self-organized micro-dimples by the low temperature plasma nitriding work as an oil pocket to preserve thin, continuous lubricating oil film between the micro-textured tool surface and the work. The measured friction coefficient remains to be low by $\mu = 0.1$. The pico-second laser micro-texturing provides a means to control the geometric dimension, the density and the alignment of micro-dimples. Higher micro-texture density in the contact track with the well-defined micro-texture geometry lowers the friction coefficient down to 0.08 with indifference to the sliding velocity.
The plasma printing becomes an alternative micro-texturing method to fabricate the fine, micro-grooved molds as well as the accurate micro-pillared DLC-coated die and to transcribe these micro-groove and micro-pillar textures into the plastic products and the metallic sheets. The contact angle for pure water is directly controlled by this micro-texturing into the plastic product. The heat transfer processes in radiation and two-phase convection are also controllable by the micro-cavity patterns in the metallic sheets.

## Acknowledgements

The author would like to his gratitude to Prof. K. Dohda (Northwestern University), Prof. N. Ono (SIT), Mr. T. Inohara (LIPS-Works, Co. Ltd.) and Mr. Y. Sugita (YS-Electric Industry, Co. Ltd.) for their help in experiments and discussion. This study is financially supported in part by MEXT-project and MITI-project, respectively.

## References

1) H. Czichos, K.-H. Habig: *Tribologie-Handbuch (Tribology handbook)*. 2nd Edition Vieweg Verlag, Wiesbaden. 2003.
2) S. Kataoka, J. Kihara, T. Aizawa: *Micro-pool mechanism in the ironing process*. Sosei-to-Kako. 30 (342), 1989, 1058-1063.
3) B. Denkena, et al.: *Efficient machining of micro-Dimples for friction reduction*. Proc. 6th ICOMM, 2012, 33-40.
4) H. Morita, T. Aizawa, N. Yoshida, S. Kurozumi: *Dry transfer stamping by nano-laminated DLC-coated tools*. Proc. 10th International Conference on Technology of Plasticity. 2012, 1103-1107.
5) E. Hosono, Hs. Zhou: *Super-hydrophobicity by Nano-pillar structuring*. Research Hot-Line. AIST 2006, 26-27.
6) P. J. Hesketh, J. N. Zemel ： *Organ pipe radiant modes of periodic micro-machined silicon surfaces*. Nature Publishing Group. 1986
7) T. Aizawa, H. Morita, T. Inohara: *Micro-dimple texturing for semi-dry stamping dies*. Proc. 11th 4M/IWMF (Denmark, 2016) (in press).
8) T. Aizawa, T. Iohara: *Micro-texturing onto glassy carbon substrates by multi-axially controlled pico-second laser machining*. Proc. 7th International Conference on Micro-Manufacturing. 2012, 66-73.
9) T. Aizawa, T. Inohara: *Multi-dimensional micro-texturing and its fabrication systems*. JP-5953198, Registered at 2016/6/17. 2016.
10) T. Aizawa, H. Suga, T. Kato, L.U. L-Silva, T. Yamaguchi: *Plasma nitriding assisted micro-texturing*. Research Report, SIT, 59 (1), 2015, 9-18.
11) T. Aizawa, K. Wasa, H. Tamagaki: *Plasma oxidation printing of micro-textures into DLC coated products*. Research Report, SIT 60 (1), 2016.
12) K. Nakamae: *How to form the hydrophobic and super-hydrophobic surfaces in Industries*. Industrial Materials 44, 1996, 26-30.

13) http://www.insurtech.com/ (2016/8/5). 2016.
14) T. Katoh, T. Aizawa, T. Yamaguchi: *Plasma assisted nitriding for micro-texturing onto martensitic stainless steels*. Manufacturing Review 2 (2), 2015, 1-7.
15) T. Aizawa, T. Nagata, H. Suga, T. Yamaguchi: *Micro-texturing into AISI-SUS420 molds for injection molding via plasma nitriding. J. Micro- and Nano-Manufactur*ing. ASME. 2016.
16) E.R.G. Eckert and R.M. Drake: *Introduction to the transfer to heat and mass*. McGraw-Hill. 1959
17) H. Yugami, Japanese Patent #2010-27831, 2010.
18) T. Aizawa, et al.: *Fabrication of mini heat-sink by the pin-injection gate die-casting*. MITI-Report. 2015
19) T. Aizawa, M. Tamaki, T. Fukuda: *Large area micro-texture imprinting onto metallic sheet via CNC stamping*. J. Procedia Engineering. 81, 1427-2432, 2014.
20) T. Aizawa, T. Fukuda: *Pulsewise motion controlled stamping for micro-texturing onto aluminum sheet*. J. Micro- and Nano-Manufacturing. ASME, 3 4-7, 2015.
21) T. Aizawa, S. Amano, H. Tamagaki: *Micro-texturing into thick DLC films for fabrication of micro-Stamping dies*. Proc. 8th AWMFT. J2, 1-6, 2015.